Synthesis and optimized formulation for high-capacity manganese fluoride (MnF2) electrodes for lithium-ion batteries

Antonin Grenier, Ana-Gabriela Porras-Gutierrez, Antoine Desrues, Sandrine Leclerc, Olaf Borkiewicz, Henri Groult, Damien Dambournet

▶ **To cite this version:**

Antonin Grenier, Ana-Gabriela Porras-Gutierrez, Antoine Desrues, Sandrine Leclerc, Olaf Borkiewicz, et al.. Synthesis and optimized formulation for high-capacity manganese fluoride (MnF2) electrodes for lithium-ion batteries. Journal of Fluorine Chemistry, 2019, 224 (Août 2019), pp.45-51. 10.1016/j.jfluchem.2019.05.007 . hal-02138390

HAL Id: hal-02138390

https://hal.sorbonne-universite.fr/hal-02138390v1

Submitted on 24 May 2019

HAL is a multi-disciplinary open access archive for the deposit and dissemination of scientific research documents, whether they are published or not. The documents may come from teaching and research institutions in France or abroad, or from public or private research centers.

L'archive ouverte pluridisciplinaire **HAL**, est destinée au dépôt et à la diffusion de documents scientifiques de niveau recherche, publiés ou non, émanant des établissements d'enseignement et de recherche français ou étrangers, des laboratoires publics ou privés.

Synthesis and Optimized Formulation for High-Capacity Manganese Fluoride (MnF_2) Electrodes for Lithium-ion Batteries

Antonin Grenier[a,b], Ana-Gabriela Porras-Gutierrez[a,b], Antoine Desrues[a,b], Sandrine Leclerc[a,b], Olaf J. Borkiewicz[c], Henri Groult[a,b], Damien Dambournet[a,b*]

[a] Sorbonne Université, CNRS, Physico-chimie des électrolytes et nano-systèmes interfaciaux, PHENIX, F-75005 Paris, France

[b] Réseau sur le Stockage Electrochimique de l'Energie (RS2E), FR CNRS 3459, 80039 Amiens cedex, France

[c] X-ray Science Division, Advanced Photon Source, Argonne National Laboratory, Argonne, Illinois 60439, USA

[*] Corresponding author: damien.dambournet@sorbonne-universite.fr

Graphical abstract:

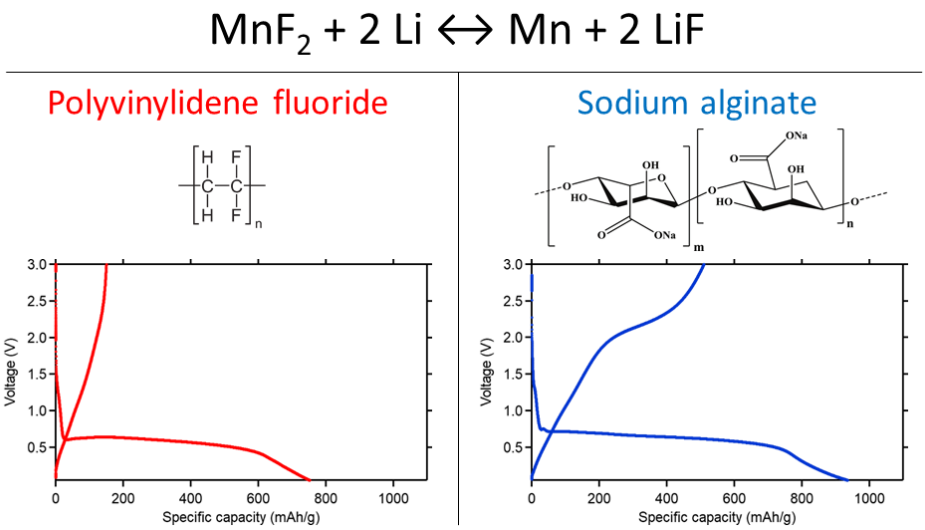

Highlights:

- Optimized solvothermal synthesis of MnF_2 targeting high reaction yield and nanosized particles.
- Investigation of ball-milling and electrode formulation as optimization routes to improve electrochemical activity of MnF_2 in Li cells.
- Aqueous formulation using sodium alginate as binder provides significant improvement of the electrochemical performance.
- Alginate-based formulation is an alternative route to ball-milling for augmenting electrochemical activity of metal fluorides.

Abstract: Electrochemical activity of poorly conductive metal fluorides in Li-ion batteries is contingent on their nanostructuration to reduce diffusion lengths and increase reaction kinetics. In that regard, we optimize the synthesis and electrode formulation of MnF_2 to enable sufficient electrochemical activity required to study its electrochemical conversion reaction mechanism. Solvothermal synthesis in a water–ethanol mixture (1:1 Vol.), using Mn acetate and a slight excess of hydrofluoric acid (HF), results in pure phase, nanosized (~30 nm diameter) rutile-type MnF_2 ($P4_2/mnm$). High energy ball-milling of MnF_2–carbon mixtures leads to an amorphization of MnF_2 and its partial phase transformation to the α-PbO_2-type structure, without significant improvement of the electrochemical performance. Changing the electrode binder, however, from typical polyvinylidene fluoride (PVDF) to water-soluble Na-alginate, leads to a significant improvement of the reversibility of the electrochemical reaction. We attribute this drastic improvement to the improved adherence and homogeneity of the electrode film prepared with Na-alginate.

Keywords: manganese fluoride, synthesis, lithium battery, formulation, binder, sodium alginate

1. Introduction

Owed to the promising theoretical energy densities of metal fluorides (MF_x) in Li-ion cells, the electrochemical conversion reaction of transition metal fluorides such as FeF_2[1], CoF_2[2] and CuF_2[3] has been the focus of multiple studies over the past two decades. Due to poor transport properties of MFx, efforts to optimize the synthesis and electrode preparation are required to enable their electrochemical activity. Badway et al. showed that complete reaction of FeF_3 with Li is made possible through a reduction in particle size, and formation of an intimate mixture, at the nano scale, with the carbonaceous conductive additive using ball milling.[4] Recently, Rui et al. have shown how nanosized MnF_2 offers large capacities at fast rates, over extended cycling, making it a promising anode material for high power applications[5,6]. Later, Bensalah et al. reported an elegant way to prepare hierarchical, nanostructured, MnF_2 – carbon nanotube composite which demonstrated excellent capacity retention.[7] These studies clearly show the crucial role of electrode preparation to increase the electrochemical performance of MnF_2. In that regard, we prepare nanosized MnF_2 and tune electrode preparation and composition to investigate how they impact electrochemical properties. We show that unlike other binary metal fluorides, ball milling induces a phase transition in MnF_2 and does not significantly improve the electrochemical performance. We circumvent the use of ball milling to increase the capacity by using a water based electrode formulation with sodium alginate as binder, and show a significant improvement of the electrochemical performance.

2. Results and discussion

2.1. Synthesis

Solvothermal synthesis of MnF_2 was performed using manganese acetate and HF as precursors. Synthesis conditions were optimized targeting single-phase, nano-sized MnF_2, and high reaction yield (see supporting information for details). An equal amount of ethanol and water as solvent led to the highest reaction yield and smallest crystallite size (**Figure S1** and **Table S1**). The molar F/Mn ratio was tuned from 1 to 2.1 (**Figure S2**). The yield of the reaction scaled with the increase of the F/Mn molar ratio which ruled out the stabilization of a significant amount of hydroxide substituting fluoride anions. The typical X-ray diffraction (XRD) pattern of the as-synthetized MnF_2 is shown in **Figure 1**. All peaks can be indexed by a tetragonal rutile-type structure ($P4_2/mnm$). Pawley refinement results in lattice parameters of a = b = 4.876(1) and c = 3.3058(1) Å, in good agreement with values previously reported by Rui et al (a = b = 4.8766 Å and c = 3.3078 Å).[6]

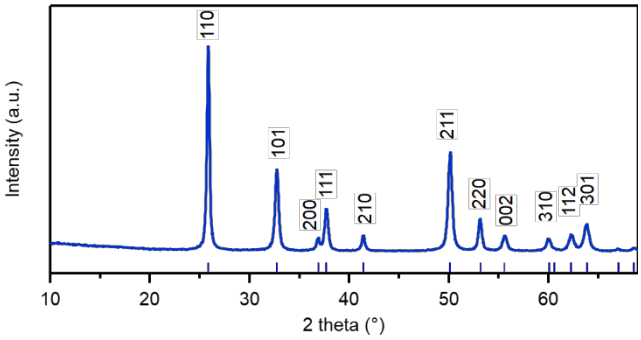

Figure 1. XRD pattern (λ = 1.5418 Å) of MnF_2 synthetized in optimized conditions (water/ethanol vol. ratio of 1, F/Mn mol. ratio of 2.1). All peaks are indexed in the $P4_2/mnm$ space group.[8]

The morphology of the MnF_2 particles was investigated using transmission electron microscopy (**Figure 2**). The particles appear monocristallized with diameters ranging from 20 to 30 nm, which is in good agreement with the estimated mean crystallite size of ~30 nm calculated from the 110 XRD peak width using Scherrer's equation. The lattice fringes observed in **Figure 2** correspond to an inter-reticular distance of 3.45 Å, which is attributed to the 110 reflection d-spacing value of 3.44 Å obtained from the Pawley refinement.

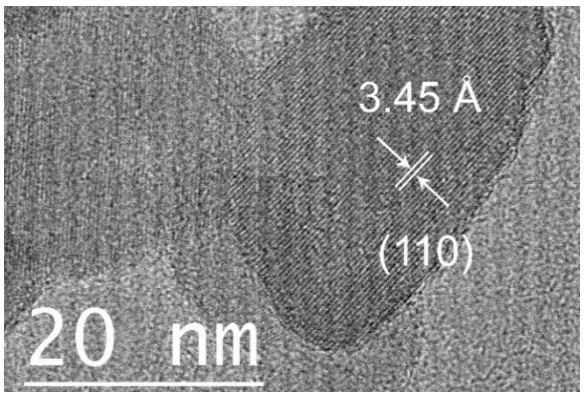

Figure 2. High-resolution transmission electron microscopy image of MnF_2 particles.

2.2. Impact of ball-milling

Ball-milling of mixtures of metal fluorides and carbon is a common method to prepare nanometric MF_x-C composites enabling electrochemical activity of MF_x insulators.[9] In this regard, we explored the impact of ball-milling on the structural and morphological features of MnF_2. XRD analysis of ball-milled MnF_2 shows a broadening of Bragg peaks and the appearance of new peaks (**Figure 3**). The latter were indexed with another type of MnF_2 polymorph having the α-PbO_2 type structure (orthorhombic, *Pbcn*).[10] The formation of this new MnF_2 phase upon ball-milling has previously been reported.[11] α-PbO_2 type structure can be considered as intermediate between the rutile and α-$PbCl_2$ (cotunnite) type structures, the latter forming at elevated pressure. The two MnF_2 polymorphs we observe present close formation energies, with the rutile type structure being more stable than the α-PbO_2 type structure by only 4 meV,[12] so that the milling process provides enough energy (pressure) to partially change the structure.

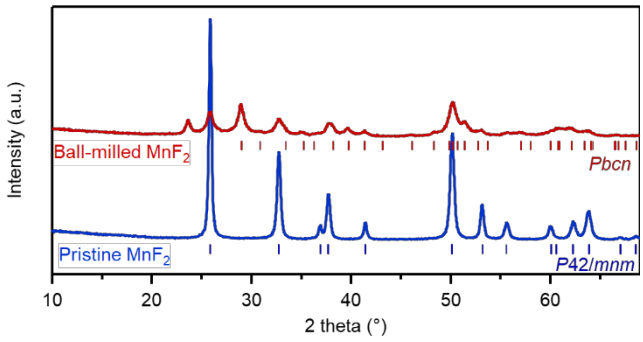

Figure 3. XRD pattern (λ = 1.5418 Å) of MnF_2 before and after ball-milling treatment. New reflections can be indexed by the PbO_2-type structure (Pbcn).[13]

To investigate the atomic structure of the milled MnF_2, we turned to pair distribution function (PDF) analysis. The PDF represents the probability, denoted G(*r*), of finding atoms separated by a distance denoted *r*.[14] PDF can probe the short to long-range order and is therefore particularly suited to study nanostructured, disordered systems.[15–17] We refined the PDF data of the ball-milled MnF_2 using rutile-type (*P*42/*mnm*) and α-PbO_2-type (*Pbcn*) structural models. Refined parameters included the PDF shape damping function (sp diameter) that corresponds to the mean scattering domain for a given phase. **Figure 4** shows the results of the refinement with a good weighted reliability factor R_w of 0.139. **Table 1** gathers the structural parameters obtained from the refinement. Overall, the structural features match literature data. The milling process does not change the lattice parameters of rutile-type MnF_2, which are identical to the ones obtained in the as synthetized sample, but reduces the coherent length (*i.e.*, crystallite size) from about 30 nm to 10 nm. To better visualize the structural difference between the two MnF_2 polymorphs, we plotted on **Figure 4** the contribution of each phases to the PDF data. The local structure of both phases is closely related. It was shown that both phases share common structural unit.[18,19] Rutile-type structure features chains of edge sharing MnO_6 octahedra with each edge-shared oxygen being corner-shared with an adjacent MnO_6 chain. In the high pressure PbO_2-type phase, the

infinite edge-sharing columns become zig-zagged with edge-shared oxygens further sharing one corner with an adjacent chain **(Figure S3)**. Note that attempts (increase of milling time, use of smaller grinding balls, use of solvents, addition of carbon black) to fully convert the rutile into the α-PbO_2 type structure failed with the systematic presence of the rutile-type structure, in agreement with previous work.[11]

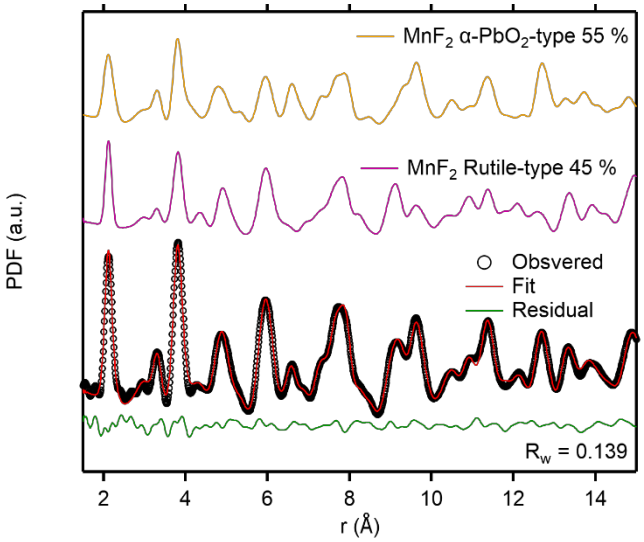

Figure 4. PDF refinement of MnF_2 ball-milled at 600 rpm for 30 min.

Table 1. Structural parameters obtained from the PDF refinement of MnF_2 ball milled at 600 rpm for 30 min. Estimated standard deviations obtained from PDFgui are given in parenthesis.

Refined parameters	Rutile-type (*P*42/*mnm*)	α-PbO_2-type (*Pbcn*)
Unit cell parameters (Å)	$a = b = 4.876(2)$ $c = 3.306(2)$	$a = 4.934(5)$ $b = 5.835(7)$ $c = 5.373(5)$
Cell volume per formula unit ($Å^3$)	39.30 (2 units per cell)	38.67 (4 unit per cell)
Coherent length (Å)	108.19(2)	86.199(1)
Scale factor ratio	0.45(3)	0.55(3)

We evaluated the effect of ball milling MnF_2 with carbon black on the electrochemical performance using a typical formulation based on polyvinylidene fluoride (PVDF) binder. An electrode where MnF_2 is manually mixed with carbon black is used as benchmark. The first few galvanostatic curves and cyclability of the two electrodes are displayed in **Figure 5**. The electrochemical profile we observe is similar to the one observed in literature, albeit with lower specific capacities in our case.[5] Ball-milling does not significantly improve the electrochemical performance, except for a better capacity retention upon extended cycling. For both electrodes, the first cycle discharge capacity of 750-800 $mAh \cdot g^{-1}$ is

larger than the theoretical capacity of MnF_2, which is 577 mAh·g^{-1} for 2 electrons exchange in the alleged electrochemical reaction shown **Equation 1**.

Equation 1. $MnF_2 + 2\ Li \leftrightarrow Mn + 2\ LiF$ $\quad E° = 1.913$ V *vs.* Li^+/Li

This larger discharge capacity can be attributed to contributions of side reactions such as solid electrolyte interface (SEI) formation, as well as activity of surface-adsorbed species (H_2O and –OH groups) forming partially reversible LiH/LiOH compounds at low voltage.[20]

Subsequent charge offers a capacity < 200 mAh·g^{-1}, resulting in a low Coulombic efficiency (CE). CE gradually increases in the following cycles, probably due to additional SEI formation in the following cycles, as well as a result of the formation of inactive domains of MnF_2 upon cycling, inferred from the progressive loss of capacity. After 40 cycles, specific capacity of the ball milled sample is ~140 mAh·g^{-1}, which is twice as much as for the manually mixed sample. This improvement can be attributed to reduced particle size of MnF_2, and its better contact with the carbon black compared to the manually mixed sample.

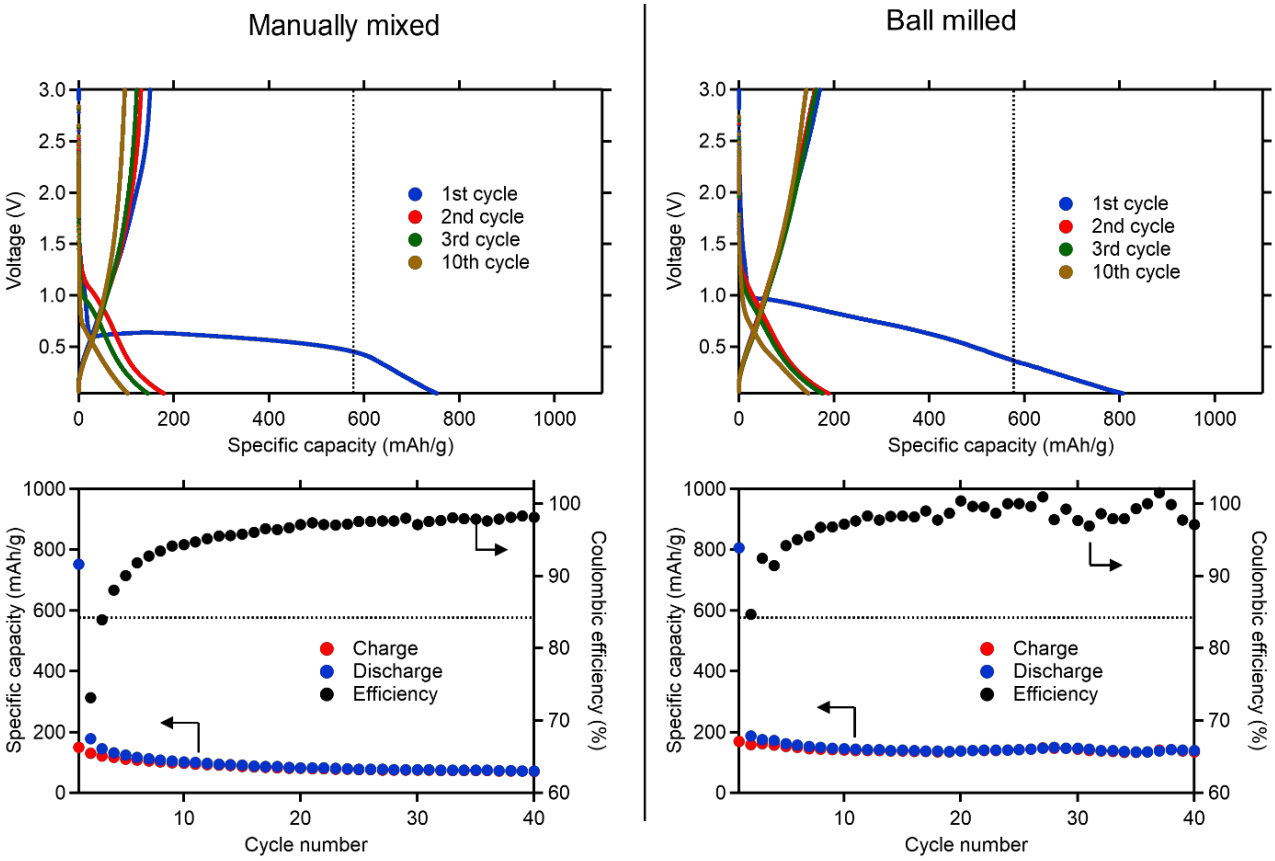

Figure 5. Comparison of galvanostatic cycling (C/10 between 3 V and 0.05 V) for electrodes prepared by manually mixing or ball milling MnF_2 and carbon black. Formulation for both electrodes is MnF_2:carbon black:PVDF 8:1:1 wt. %. Dashed lines mark the value of the theoretical capacity of MnF_2 (577 mAh·g^{-1}).

Surprisingly, the ball milling process is not accompanied by a significant increase of the capacity in the early stage of cycling, as previously reported for FeF_3 in similar milling conditions.[4] Attempts to optimize the milling process in dry conditions (ball size, duration, rotational speed) did not significantly improve the electrochemical performance. However, ball milling in wet conditions and at low speed – particularly with viscous solvent 1-octanol – provides a significant improvement of the specific capacity (**Figure 6**).

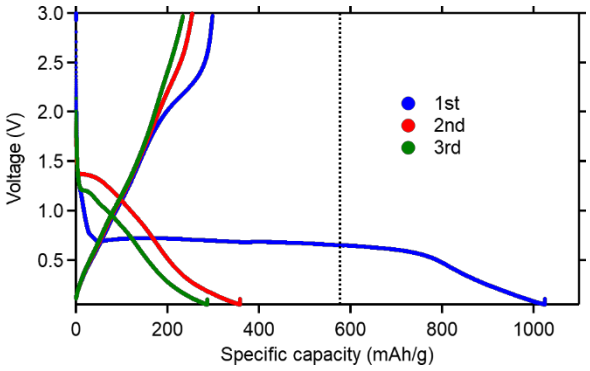

Figure 6. First 3 cycles of galvanostatic cycling (C/10 between 3 V and 0.05 V) for electrodes prepared by wet ball-milling of a mixture of MnF_2 and carbon black (90:10 wt. %) in 1-octanol at 100 rpm for 1 h.

In these mild conditions, the phase transformation of MnF_2 is suppressed (**Figure S4**). It is unclear if the phase transformation of MnF_2 is detrimental to the electrochemical performance, as the improvement of the specific capacity observed here may be solely due to a more intimate MnF_2:C mixture.

2.3. Optimization of the formulation and electrochemical behavior

In an effort to further improve the electrochemical performance, we focused on the impact of the nature of the polymer binder, a key component in the electrode fabrication.[21] The objective was to increase the specific capacity and reduce capacity fading in hope of studying the conversion mechanism. We chose an aqueous formulation using sodium alginate as binder as it showed promise in Si-based alloying anodes.[22]

Scanning electron microscopy (SEM) of the two films prepared using Na-alginate and PVDF is shown **Figure 7**. In the case of PVDF, the electrode film is not homogenous with the presence of large micrometer-size aggregates of MnF_2 particles. On the other hand, the use of an aqueous-based slurry and alginate as binder leads to a more homogenous film.

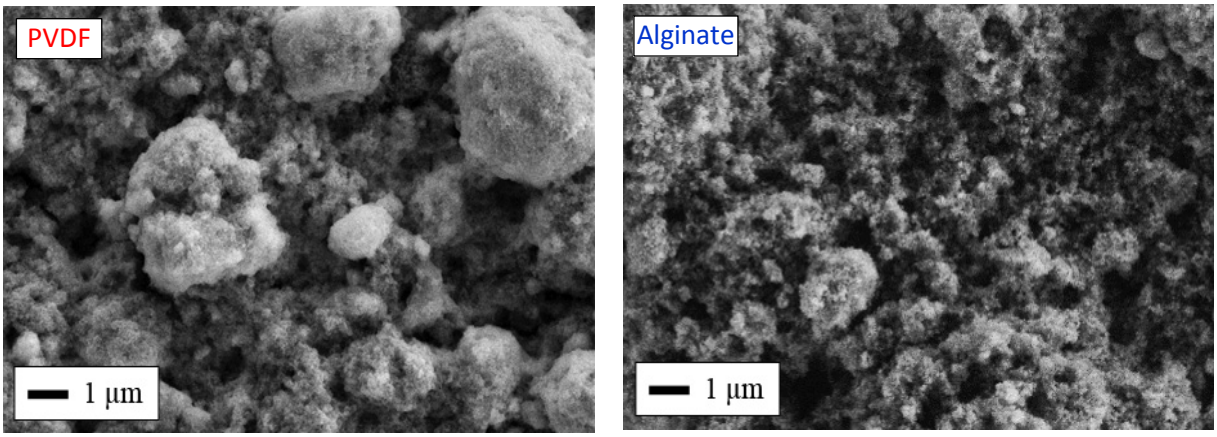

Figure 7. Representative scanning electron micrographs of the surface of electrodes prepared using either PVDF (left), or alginate (right), as the binder.

Comparison of XRD patterns recorded after preparation of the two electrodes suggest that the aqueous preparation does not appreciably change the structure of MnF_2 (**Figure S5**). All peaks can be indexed by rutile-type MnF_2, with additional low intensity peaks attributable to Cu from the current collector, which was inadvertently scraped off during sample preparation. A representative energy dispersive X-ray (EDX) spectrum recorded on the Na-alginate-based electrode shows peaks characteristic of Mn, F, C, O and Cu (**Figure S6**).

The improved homogeneity of the MF_x-C composite is reflected in a significant improvement in the electrochemical activity of MnF_2. **Figure 8** shows results of galvanostatic cycling of MnF_2 electrodes prepared with alginate. The aqueous formulation provides a substantial improvement of the reversibility of the reaction, with a major increase of the 1st charge capacity (~500 mAh·g^{-1}) compared to the electrode prepared with PVDF (~150 mAh·g^{-1}) in comparable conditions.

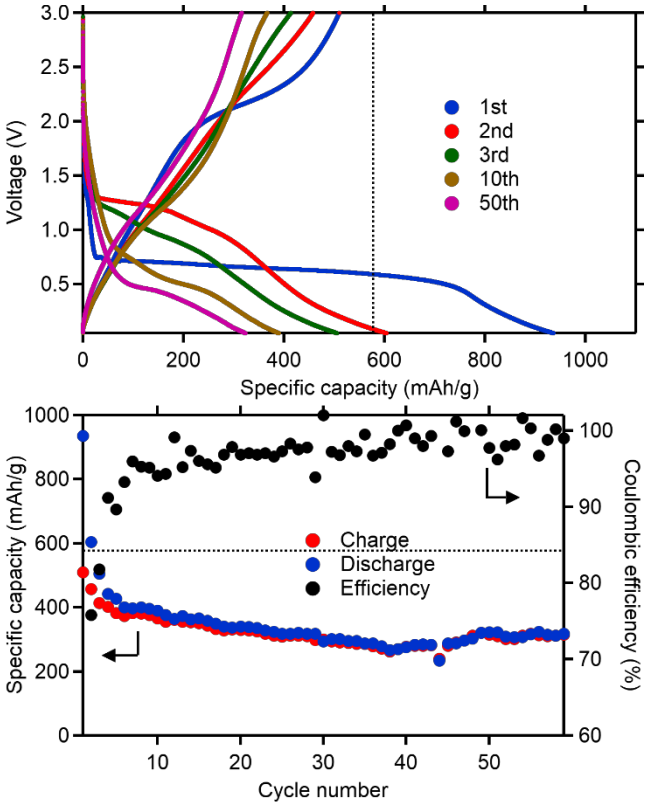

Figure 8. Galvanostatic cycling (C/10 between 3V and 0.05 V) of MnF_2 electrodes prepared using sodium alginate as binder. Formulation is MnF_2:carbon black:Na-Alginate 8:1:1 wt. %. Dashed lines mark the value of the theoretical capacity of MnF_2 (577 $mAh \cdot g^{-1}$).

The contribution of the carbon black and alginate additives to the improved performance provided by the aqueous formulation was evaluated by preparing an electrode without MnF_2 (**Figure S7**). The stable extra capacity provided by the additives past the 1st discharge (130–140 $mAh \cdot g^{-1}$, expressed as a function of the mass of carbon black) corresponds to an extra capacity of 14–16 $mAh \cdot g^{-1}$ in the MnF_2-containing electrode. This contribution is larger in the first discharge (29 $mAh \cdot g^{-1}$), where SEI formation principally occurs. These additive-generated extra capacities are well below the capacities we measure in the actual MnF_2-containing electrode, showing that the substantial increase of the capacities originates from an improved electrochemical activity of MnF_2 in the alginate-based formulation. We believe this improvement is largely provided by the more intimate contact between MnF_2 and carbon black in the composite electrode. Water may favor dispersion of carbon and MnF_2 in the slurry, resulting in a more homogeneous mixture of the two in the dried electrode. Increased amount of adsorbed OH and H_2O groups on the surface of MnF_2, incurred by the aqueous-based slurry preparation, might also contribute to these larger capacities.[20] These surface species may also provide improved binding with the alginate carboxy/hydroxy groups *via* hydrogen bonds.[23]

The dramatic changes occurring during discharge ($I < 0$) are characterized by a large cathodic peak centered at ~ 0.4 V on the cyclic voltammetry recorded on the alginate-based MnF_2 electrode (**Figure**

9). Considering the standard potential of ~1.9 V calculated from reaction depicted **Equation 1**, this result in an apparent 1.5 V overpotential, above the typical values (~1 V) of conversion reactions involving metal fluorides and their relatively strong M–F bonds.[25]

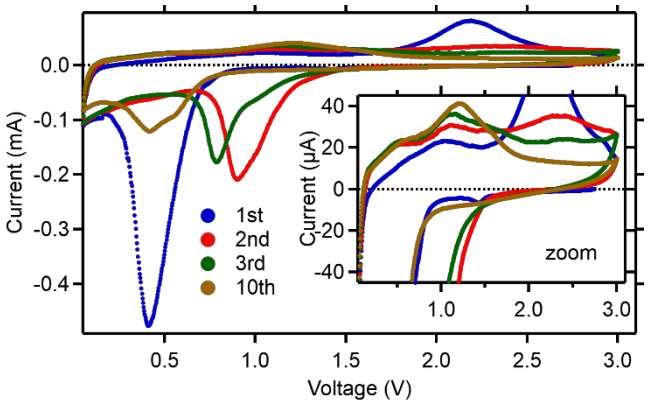

Figure 9. Cyclic voltammetry (0.05 – 3 V at 0.04 $mV \cdot s^{-1}$) of MnF_2 electrodes prepared using sodium alginate as binder. Formulation is MnF_2:carbon black:Na-Alginate 8:1:1 wt. %.

In the second cycle, the cathodic current is smaller and shifted to higher voltage. The smaller current observed in the second discharge current can be attributed to the formation of the SEI that is expected to predominantly occur in the first discharge. The shift of the cathodic peak to a higher voltage of about 1 V, reducing the apparent overpotential to ~0.9 V, suggests that the resistance of the electrochemical reaction is reduced—in other words, the dramatic structural changes occurring in the first discharge seem to facilitate the reaction in the subsequent cycle. After the second discharge and upon subsequent cycling, the resistance of the reaction increases: the cathodic current continues to decrease (i.e., the electrode reacts less) and now shifts to lower voltage (i.e., the overpotential increases), suggesting a degradation of the electrode. Surprisingly, there is a distinct asymmetry of the cathodic peak after the first discharge that persists during cycling, suggesting that at least two different electrochemical processes are taking place.

The charge ($I > 0$) also features at least two distinct anodic peaks in the 1.0–1.2 V and 2.2–2.4 V ranges, further suggesting that multiple redox processes are taking place in this potential range. Overall, electrochemical reactions seem to shift to lower potential upon further cycling, suggesting a change in the electrochemical reaction pathway.

2.4. Microscopic observations

Figure 10 shows representative TEM images of electrodes before and after electrochemical reactions and illustrates the dramatic morphological and structural changes occurring upon discharge. The conversion process of the pristine MnF_2 particles (**Figure 10.A2**) leads to formation of smaller domains

of about 2 nm in diameter, which are characterized by a darker image contrast. These smaller domains seem embedded within the original MnF_2 particles (**Figure 10.B2**). Based on literature, we presume these domains correspond to metallic manganese, supposedly in its low temperature allotropic form α-Mn (*I*-43*m*), and are embedded in a LiF matrix.[6] Here, fast Fourier transform (FFT) analyses of the small darker-contrast domains results in large uncertainties in d-spacing values, so that we can't differentiate between reflections of MnF_2, α-Mn and LiF. It is interesting to note that we observe smaller darker contrast domains compared to TEM studies by Rui et al.[6] on larger MnF_2 particles (100–300 nm diameter), where darker contrast domains are 10–15 nm in diameter. This observation suggests that the size of the Mn domains are proportional (roughly 10 times smaller) to the size of the original MnF_2 particle in which they form. If migration of Li^+ principally occurs at the Mn–LiF interface, and considering the increased area of the Mn–LiF interface produced by smaller Mn domains, nanostructuration may therefore further improve reaction kinetics in addition to simple reduction of diffusion lengths. Essentially, this observation suggests that smaller particles would lead to smaller metallic domains, which would in turn lead to faster bulk transport.

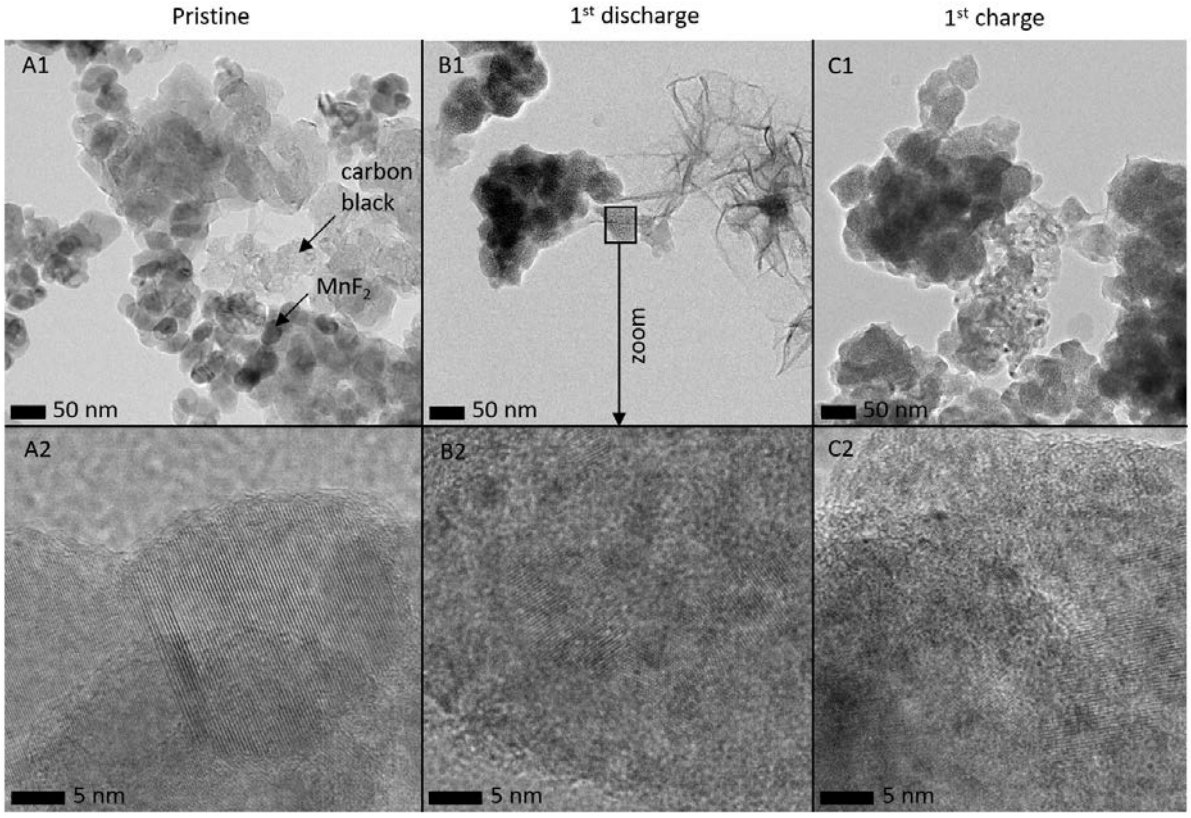

Figure 10. TEM images of MnF_2:carbon black:Na-alginate electrodes in a 8:1:1 wt. ratio (A) pristine, (B) after the first discharge and (C) after the first charge. The 1 and 2 indices represent two different magnifications of the same electrode. Regions displayed in images 2 are not necessarily visible in images 1.

Subsequent charge does not dramatically change the morphology of the MnF_2 particles, where darker contrast domains subsist, as some Mn regions likely become inactive after the first discharge.

Conclusions

In conclusion, we show an alternative route to ball-milling to prepare electrochemically active MnF_2–C nanocomposites using alginate as binder. The MnF_2 electrode prepared with the alginate-based aqueous formulation shows a significant improvement of the electrochemical performance over an electrode prepared with the typical PVDF in NMP formulation. The increased reversibility may be explained, at least partially, by the more intimate MnF_2–C mixture which offers better electronic transport in the electrode. Significant changes in the electrochemical profile, characterized by major shifts of redox peaks in cyclic voltammograms during the first 10 cycles, suggest that the reaction pathway of the alleged electrochemical mechanism $MnF_2 + 2\ Li \leftrightarrow Mn + 2\ LiF$ is changed within the first few cycles. TEM micrographs of an MnF_2 electrode after the first discharge show major structural changes occurring within the ~30 nm MnF_2 particles. The conversion reaction results in the formation of smaller particles of darker contrast – expected to be metallic Mn – within the original MnF_2 particles. Comparison with literature suggest that the Mn domains formed are dependent on the size of the original MnF_2 particles.

3. Experimental

4.1. Synthesis

$Mn(CH_3COO)_2.4H_2O$ (99 %, Aldrich) and HF (40 %, Prolabo) were used as precursors for solvothermal synthesis in polytetrafluoroethylene-lined stainless steel pressure vessels. In a typical synthesis, 2.637 g of $Mn(CH_3COO)_2.4H_2O$ was dissolved in 14.5 mL of deionized (DI) water. Subsequently, 14.5 mL of ethanol was added followed by 1 mL of HF corresponding to a molar ratio F/Mn equals to 2.1. Light pink MnF_2 particles instantly precipitated. The total volume of the solution was fixed to 30 mL in the 50 mL liner. The mixture was heated at 90 °C for 12 hours. The autoclave was cooled down to room temperature before being opened. The supernatant was then removed and ethanol (about 20 mL) was poured under stirring to wash the obtained product. The suspension was then transferred into a polyflor centrifuge tube and centrifuged at 4400 rpm for 15 min. Supernatant ethanol was removed and the tube was placed in an oven at 80 °C for 2 hours in order to dry the powder. Finally, the powder was further outgassed at 150 °C for 12 hours under vacuum.

4.2. Carbon metal fluoride composite preparation

Ball milling was performed in ambient conditions using a planetary ball mill (FRITSCH Pulverisette 7 premium line), using ZrO_2 grinding balls (10 mm diameter) and jars (20 mL). 300 mg of MnF_2 was milled at 600 rpm for 30 min with 5 min pause every 15 min. Milling with the addition of carbon black (Pure Black, Superior Graphite) for preparation of electrodes did not show any appreciable change in the structure of MnF_2. Wet ball-milling of the MnF_2 and carbon black mixture (90:10 wt. %, 300 mg) was performed in 2 mL of 1-octanol (Sigma-Aldrich, anhydrous, ≥ 99 %) at 100 rpm for 1 h using the

same ZrO_2 balls and jars. The resulting slurry was dried at 80 °C under vacuum overnight before electrode preparation.

4.3. Characterizations

MnF_2 powder's morphology and composition was studied using a high-resolution transmission electron microscope (HRTEM, JEOL JEM 2011) equipped with an energy dispersive X-ray spectrometer (EDX, PGT IMIX), and a scanning electron microscope (SEM, Zeiss EVO MA10). For TEM, a drop of a suspension of the powder (as prepared MnF_2 or scraped electrode) in ethanol was deposited on a copper grid covered with carbon. For SEM, electrodes were used as is. Laboratory XRD (Rigaku Ultima IV, Cu-Kα radiation) was used to characterize the phase of the obtained powder. Crystallite size was estimated using Scherrer's method implemented in MDI JADE. Pawley refinement was performed with TOPAS v5. Background was fit using a linear interpolation between 6 points. Peak-shape profile was fit using the TCHz pseudo-Voigt function implemented in TOPAS.

Synchrotron X-ray diffraction data suited for pair distribution function (PDF) analysis were collected at the 11-ID-B beamline at the Advanced Photon Source at Argonne National Laboratory, using high energy X-rays ($\lambda = 0.2128$ Å) at $Q_{max} \approx 22$ Å^{-1}.[26,27] Powders were loaded in polyimide tubing (Cole-Parmer) sealed with epoxy glue. One-dimensional diffraction data were obtained by integrating the 2D images in Fit2D.[28] PDFs, G(r), were calculated with appropriate corrections (e.g. Compton scattering) using PDFgetX2 or PDFgetX3.[29] The PDFs were subsequently modeled using PDFgui.[30] Refined parameters included scale factor, lattice parameters, atomic displacement parameters (ADP, different for Mn and F, but isotropic as to limit the number of parameters), atomic positions, spdiameter (dampening factor due to limited coherent length/crystallite size), and delta1 (accounts for increased amplitude of 1st peak due to correlated motion of neighboring atoms). Instrumental PDF dampening parameter Q_{damp} was fixed to 0.04. Although PDF is presented in limited r ranges, the weighted reliability factor R_{wp} values we report are for refinement in the 1.5–60 Å range.

4.4. Electrochemistry

The electrochemical properties of MnF_2 were evaluated in CR2032 coin cells. Unless specified otherwise, MnF_2 (80 wt. %) was mixed with graphitized carbon black (ref 205-110 "Pure Black",[31] Superior Graphite, 10 wt%) and a polymer binder (10 wt. %). The latter was either polyvinylidene fluoride (PVDF, Aldrich) or sodium alginate (MTI Corp.). PVDF-based slurries were prepared using N-methyl-2-pyrrolidone (Fisher) and alginate-based slurries with deionized water. The slurries were tape cast onto copper foil (99.99 %, MTI Corp.) with a doctor blade and dried for 2 h at 70 °C in an oven. 10 mm electrodes were punched, calendered between two pieces of copper, and dried overnight at 100 °C under vacuum. Mass loading ranged from 1.4 to 2.3 mg of MnF_2 per cm^2 of electrode. Coin cells were assembled in argon filled glove box using lithium foil (99.9%, Aldrich) and Celgard separator soaked

in 1 M $LiPF_6$ dissolved in an ethylene carbonate and dimethyl carbonate (1:1 Vol. %, Merck). Galvanostatic cycling was performed between 0.05 and 3 V, at 30 $mA \cdot g^{-1}$, using a BST8-WA system from MTI Corp or a VMP3 system from Bio-Logic. Cyclic voltammetry was recorded between 0.05 and 3 V at 0.04 $mV \cdot s^{-1}$ on a VMP3 potentiostat from Bio-Logic.

Acknowledgements

We thank S. Casale for HRTEM analyses. The work done at the Advanced Photon Source, an Office of Science User Facility operated for the U.S. Department of Energy (DOE) Office of Science by Argonne National Laboratory, was supported by the U.S. DOE under Contract No. DE-AC02-06CH11357.

References

[1] F. Wang, R. Robert, N.A. Chernova, N. Pereira, F. Omenya, F. Badway, X. Hua, M. Ruotolo, R. Zhang, L. Wu, V. Volkov, D. Su, B. Key, M. Stanley Whittingham, C.P. Grey, G.G. Amatucci, Y. Zhu, J. Graetz, Conversion reaction mechanisms in lithium ion batteries: Study of the binary metal fluoride electrodes, J. Am. Chem. Soc. 133 (2011) 18828–18836. doi:10.1021/ja206268a.

[2] Y.T. Teng, S.S. Pramana, J. Ding, T. Wu, R. Yazami, Investigation of the conversion mechanism of nanosized CoF_2, Electrochim. Acta. 107 (2013) 301–312. doi:10.1016/j.electacta.2013.05.107.

[3] X. Hua, R. Robert, L.-S. Du, K.M. Wiaderek, M. Leskes, K.W. Chapman, P.J. Chupas, C.P. Grey, Comprehensive Study of the CuF_2 Conversion Reaction Mechanism in a Lithium Ion Battery, J. Phys. Chem. C. 118 (2014) 15169–15184. doi:10.1021/jp503902z.

[4] F. Badway, F. Cosandey, N. Pereira, G.G. Amatucci, Carbon Metal Fluoride Nanocomposites, J. Electrochem. Soc. 150 (2003) A1318. doi:10.1149/1.1602454.

[5] K. Rui, Z. Wen, X. Huang, Y. Lu, J. Jin, C. Shen, High-performance lithium storage in an ultrafine manganese fluoride nanorod anode with enhanced electrochemical activation based on conversion reaction, Phys. Chem. Chem. Phys. 18 (2016) 3780–3787. doi:10.1039/C5CP07361H.

[6] K. Rui, Z. Wen, Y. Lu, J. Jin, C. Shen, One-Step solvothermal synthesis of nanostructured manganese fluoride as an anode for rechargeable lithium-ion batteries and insights into the conversion mechanism, Adv. Energy Mater. 5 (2015). doi:10.1002/aenm.201401716.

[7] N. Bensalah, D. Turki, F.Z. Kamand, K. Saoud, Hierarchical Nanostructured MWCNT-MnF_2 Composites With Stable Electrochemical Properties as Cathode Material for Lithium Ion Batteries, Phys. Status Solidi. 215 (2018) 1800151. doi:10.1002/pssa.201800151.

[8] L.M.A. da Veiga, L.R. Andrade, W. Gonschorek, The crystal structure of manganese difluoride (MnF_2): Reliability test of hypothetical intensity variances by means of χ^2 distributions, Zeitschrift Für Krist. 160 (1982) 171–178. doi:10.1524/zkri.1982.160.3-4.171.

[9] F. Badway, F. Cosandey, N. Pereira, G.G. Amatucci, Carbon Metal Fluoride Nanocomposites High-Capacity Reversible Metal Fluoride Conversion Materials as Rechargeable Positive Electrodes for Li Batteries, J. Electrochem. Soc. 150 (2003) A1318–A1327. doi:10.1149/1.1602454.

[10] S.S. Kabalkina, S. V. Popova, Phase Transitions in Zinc and Manganese Fluorides at High Pressures and Temperatures, Sov. Phys. Dokl. 8 (1964) 1141.

[11] I. Hernández, F. Rodríguez, Spectroscopic study of milled MnF_2 nanoparticles. Size-and-strain-induced photoluminescence enhancement, J. Phys. Condens. Matter. 19 (2007) 356220. doi:10.1088/0953-8984/19/35/356220.

[12] A. Jain, S.P. Ong, G. Hautier, W. Chen, W.D. Richards, S. Dacek, S. Cholia, D. Gunter, D. Skinner, G. Ceder, K.A. Persson, Commentary: The Materials Project: A materials genome approach to accelerating materials innovation, APL Mater. 1 (2013) 011002. doi:10.1063/1.4812323.

[13] S.S. Kabalkina, S. V. Popova, Phase transition in high temperatures, Dokl. Akad. Nauk SSSR. 153 (1963) 1310–1312. http://www.mathnet.ru/links/cc519b778ea442b0c08395932c395fca/dan28942.pdf.

[14] D.A. Keen, A comparison of various commonly used correlation functions for describing total scattering, J. Appl. Crystallogr. 34 (2001) 172–177. doi:10.1107/S0021889800019993.

[15] A.S. Masadeh, E.S. Božin, C.L. Farrow, G. Paglia, P. Juhas, S.J.L. Billinge, A. Karkamkar, M.G. Kanatzidis, Quantitative size-dependent structure and strain determination of CdSe nanoparticles using atomic pair distribution function analysis, Phys. Rev. B. 76 (2007) 115413. doi:10.1103/PhysRevB.76.115413.

[16] B. Shyam, K.W. Chapman, M. Balasubramanian, R.J. Klingler, G. Srajer, P.J. Chupas, Structural and mechanistic revelations on an iron conversion reaction from pair distribution function analysis, Angew. Chemie - Int. Ed. 51 (2012) 4852–4855. doi:10.1002/anie.201200244.

[17] K.M.Ø. Jensen, P. Juhas, M.A. Tofanelli, C.L. Heinecke, G. Vaughan, C.J. Ackerson, S.J.L. Billinge, Polymorphism in magic-sized $Au_{144}(SR)_{60}$ clusters, Nat. Commun. 7 (2016) 11859. doi:10.1038/ncomms11859.

[18] D.W. Meng, X.L. Wu, F. Sun, L.W. Huang, F. Liu, Y.J. Han, J.P. Zheng, X. Meng, R. Mason, High-pressure polymorphic transformation of rutile to α-PbO_2-type TiO_2 at {011}R twin boundaries, Micron. 39 (2008) 280–286. doi:10.1016/j.micron.2007.07.001.

[19] J. Wittkamper, Z. Xu, B. Kombaiah, F. Ram, M. De Graef, J.R. Kitchin, G.S. Rohrer, P.A. Salvador, Competitive Growth of Scrutinyite (α-PbO_2) and Rutile Polymorphs of SnO2 on All Orientations of Columbite $CoNb_2O_6$ Substrates, Cryst. Growth Des. 17 (2017) 3929–3939. doi:10.1021/acs.cgd.7b00569.

[20] Y.-Y. Hu, Z. Liu, K.-W. Nam, O.J. Borkiewicz, J. Cheng, X. Hua, M.T. Dunstan, X. Yu, K.M. Wiaderek, L.-S. Du, K.W. Chapman, P.J. Chupas, X.-Q. Yang, C.P. Grey, Origin of additional capacities in metal oxide lithium-ion battery electrodes., Nat. Mater. 12 (2013) 1130–6. doi:10.1038/nmat3784.

[21] S. Komaba, N. Yabuuchi, T. Ozeki, Z.-J. Han, K. Shimomura, H. Yui, Y. Katayama, T. Miura, Comparative Study of Sodium Polyacrylate and Poly(vinylidene fluoride) as Binders for High Capacity Si–Graphite Composite Negative Electrodes in Li-Ion Batteries, J. Phys. Chem. C. 116 (2012) 1380–1389. doi:10.1021/jp204817h.

[22] I. Kovalenko, B. Zdyrko, A. Magasinski, B. Hertzberg, Z. Milicev, R. Burtovyy, I. Luzinov, G. Yushin, A Major Constituent of Brown Algae for Use in High-Capacity Li-Ion Batteries, Science (80-.). 334 (2011) 75–79. doi:10.1126/science.1209150.

[23] L. Ling, Y. Bai, Z. Wang, Q. Ni, G. Chen, Z. Zhou, C. Wu, Remarkable Effect of Sodium Alginate Aqueous Binder on Anatase TiO_2 as High-Performance Anode in Sodium Ion Batteries, ACS Appl. Mater. Interfaces. 10 (2018) 5560–5568. doi:10.1021/acsami.7b17659.

[24] W.M. Haynes, CRC Handbook of Chemistry and Physics, 95th Edition, 2014-2015, 95th editi, CRC Press, Boca Raton, 2014. doi:10.1136/oem.53.7.504.

[25] Y. Oumellal, A. Rougier, G.A. Nazri, J.M. Tarascon, L. Aymard, Metal hydrides for lithium-ion batteries, Nat. Mater. 7 (2008) 916–921. doi:10.1038/nmat2288.

[26] P.J. Chupas, K.W. Chapman, P.L. Lee, Applications of an amorphous silicon-based area detector for high-resolution, high-sensitivity and fast time-resolved pair distribution function measurements, J. Appl. Crystallogr. 40 (2007) 463–470. doi:10.1107/S0021889807007856.

[27] P.J. Chupas, X. Qiu, J.C. Hanson, P.L. Lee, C.P. Grey, S.J.L. Billinge, Rapid-acquisition pair distribution function (RA-PDF) analysis, J. Appl. Crystallogr. 36 (2003) 1342–1347. doi:10.1107/S0021889803017564.

[28] A.P. Hammersley, S.O. Svensson, M. Hanfland, A.N. Fitch, D. Hausermann, Two-dimensional

detector software: From real detector to idealised image or two-theta scan, High Press. Res. 14 (1996) 235–248. doi:10.1080/08957959608201408.

[29] X. Qiu, J.W. Thompson, S.J.L. Billinge, PDFgetX2: a GUI-driven program to obtain the pair distribution function from X-ray powder diffraction data, J. Appl. Crystallogr. 37 (2004) 678. doi:10.1107/S0021889804011744.

[30] C.L. Farrow, P. Juhas, J.W. Liu, D. Bryndin, E.S. Božin, J. Bloch, T. Proffen, S.J.L. Billinge, PDFfit2 and PDFgui: computer programs for studying nanostructure in crystals., J. Phys. Condens. Matter. 19 (2007). doi:10.1088/0953-8984/19/33/335219.

[31] E. Raymundo-Piñero, M. Cadek, F. Béguin, Tuning carbon materials for supercapacitors by direct pyrolysis of seaweeds, Adv. Funct. Mater. 19 (2009) 1032–1039. doi:10.1002/adfm.200801057.

Supporting Information

Synthesis and Optimized Formulation for High-Capacity Manganese Fluoride (MnF_2) Electrodes for Lithium-ion Batteries

Antonin Grenier[a,b], Ana-Gabriela Porras-Gutierrez[a,b], Antoine Desrues[a,b], Sandrine Leclerc[a,b], Olaf J. Borkiewicz[c], Henri Groult[a,b], Damien Dambournet[a,b*]

[a] Sorbonne Université, CNRS, Physico-chimie des électrolytes et nano-systèmes interfaciaux, PHENIX, F-75005 Paris, France

[b] Réseau sur le Stockage Electrochimique de l'Energie (RS2E), FR CNRS 3459, 80039 Amiens cedex, France

[c] X-ray Science Division, Advanced Photon Source, Argonne National Laboratory, Argonne, Illinois 60439, USA

[*] Corresponding author: damien.dambournet@sorbonne-universite.fr

Optimized synthesis conditions

- *Solvents*: Preliminary syntheses in pure ethanol, pure water and a mixture of ethanol and water (1:1 Vol. ratio) were realized with a molar ratio (R) F/Mn equals to 2.1. The temperature and heating time of the solvothermal synthesis were fixed to 90 °C and 12 h. All syntheses gave pure single-phase MnF_2 with rutile-type structure (P42/mnm space group), as shown in **Figure S1**. Crystallite size estimated from Scherrer's equation from the (110) peak and the yield of the reaction are gathered in **Table S1**. The mixture of water and ethanol gave the best result: smallest crystallite size and high yield.

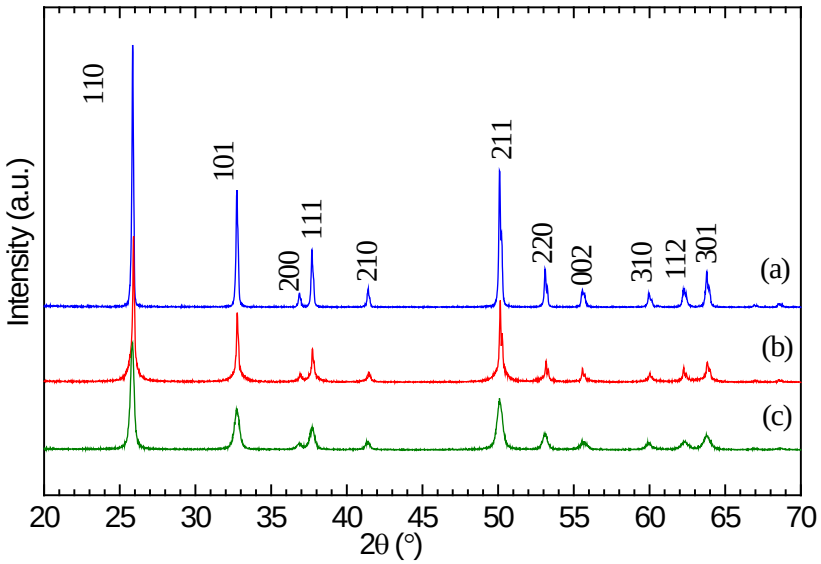

Figure S1. XRD patterns (λ = 1.5418 Å) of MnF_2 synthetized in (a) H_2O, (b) EtOH, (c) H_2O:EtOH 1:1.

Table S1. Crystallite size estimated by Scherrer's equation with the XRD's 110 peak and yield of syntheses performed in water, ethanol and the water-ethanol mixture

Solvent	Crystallite size from 110 peak (nm)	Yield (%)
H_2O	> 100	78
EtOH	68	15
EtOH:H_2O 1:1 in vol	29	99

- *F/Mn molar ratio*: Here, we used water-ethanol mixture as solvents. We defined R as the F/Mn molar ratio. This parameter was investigated as it was suspected that hydroxyfluoride composition could eventually form. The reaction temperature and duration time were fiwed at 90 °C and 12 hours.
The $R_{F/Mn}$ value was varied from 1 to 2.1. All synthesis yielded to pure single phase of MnF_2. The yield of the reaction (based on Mn) is shown **Figure S2**.

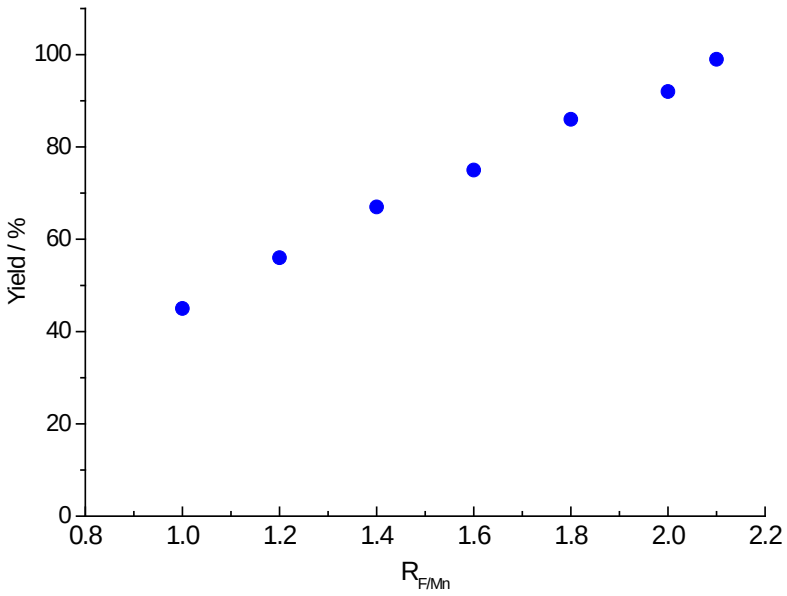

Figure S2. Evolution of the yield of the reaction as a function of the $R_{F/Mn}$ molar ratio.

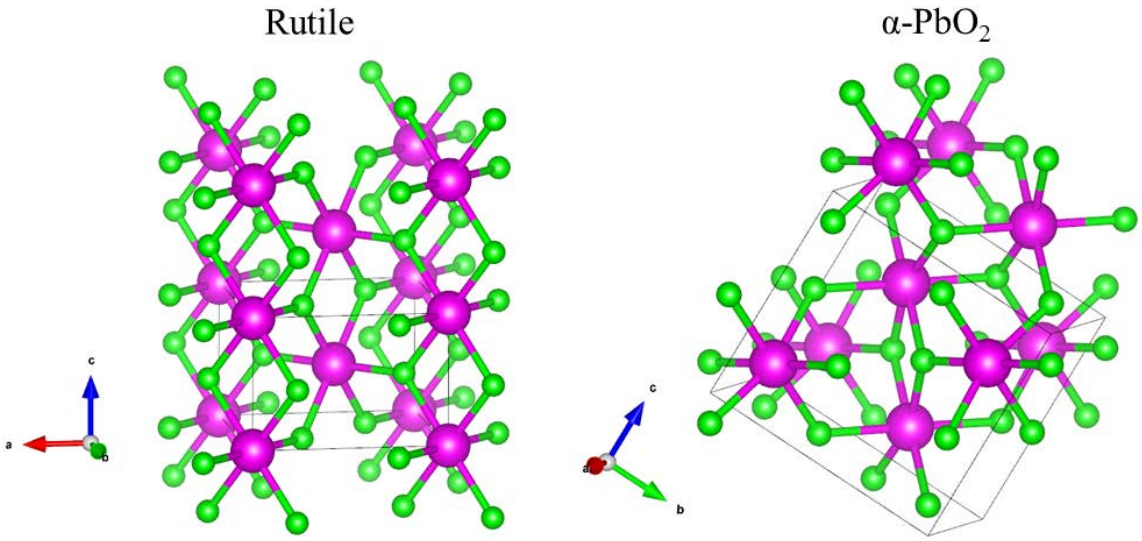

Figure S3. Structural representations of rutile and α-PbO_2 polymorphs of MnF_2.

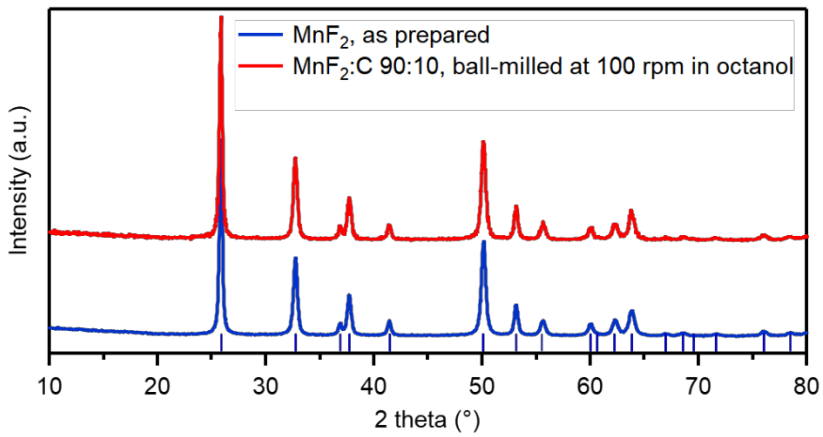

Figure S4. XRD pattern (λ = 1.5418 Å) of the dried MnF_2:C mixture (90:10 wt. %) ball-milled in 1-octanol at 100 rpm for 1 hour. The XRD pattern of as-prepared MnF_2 is shown for comparison.

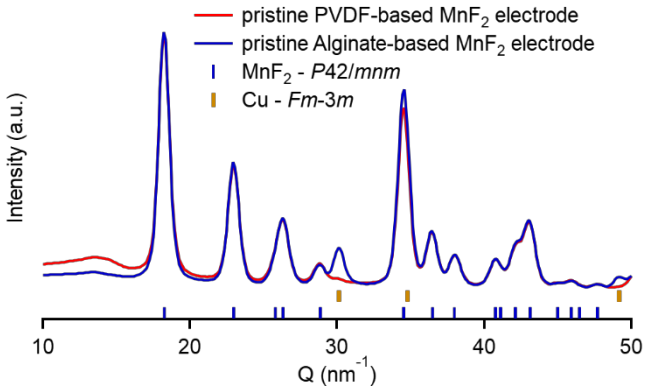

Figure S5. Synchrotron XRD patterns (λ = 0.2128 Å) recorded after preparation of the PVDF and alginate-based electrodes.

The larger amount of Cu present in the XRD pattern of the alginate-based electrode illustrates the improved adherence of the electrode film to the current collector relative to the PVDF-based electrode. It was much more difficult to scrape the alginate-based electrode off the Cu current collector.

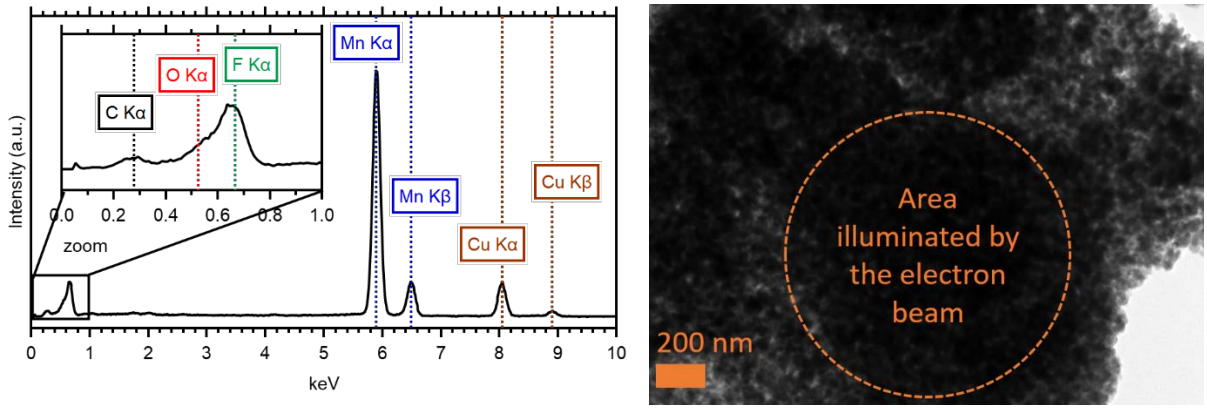

Figure S6. Energy dispersive X-ray spectrum of the pristine alginate-based MnF_2 electrode. The transmission electron micrograph shows the corresponding area illuminated by the probing electron beam.

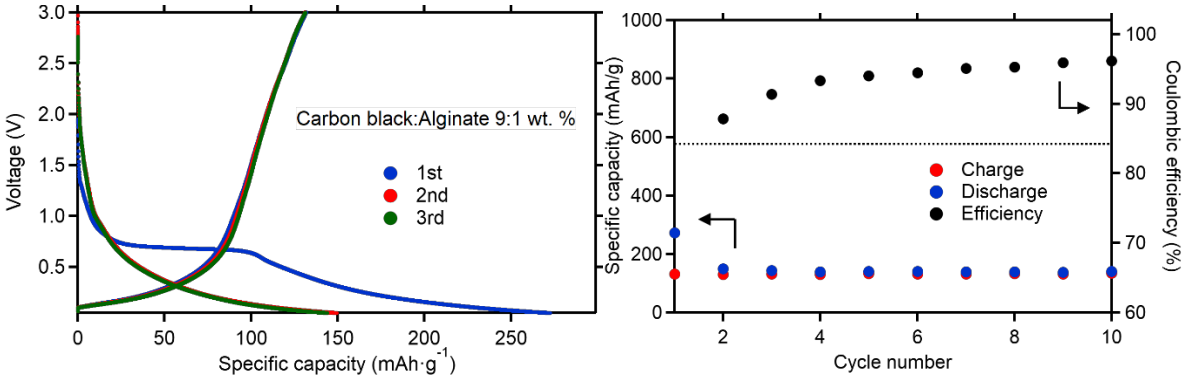

Figure S7. Galvanostatic cycling of a reference electrode without MnF_2. The current used (~24 µA) here is identical to the one employed in galvanostatic cycling of the alginate-based MnF_2 electrode presented **Figure 9** of the manuscript. This corresponds to a current density of Formulation is carbon black:Na-Alginate 9:1 wt. %. Specific capacities are expressed as a function of the mass of carbon black.